Carbohydrate Polymers 108 (2014) 192–199

Contents lists available at ScienceDirect

Carbohydrate Polymers

journal homepage: www.elsevier.com/locate/carbpol

Electrospun nanofibrous chitosan membranes modified with polyethyleneimine for formaldehyde detection

Na Wang[a], Xianfeng Wang[a], Yongtang Jia[b], Xiaoqi Li[c], Jianyong Yu[d], Bin Ding[a,d,*]

[a] State Key Laboratory for Modification of Chemical Fibers and Polymer Materials, College of Materials Science and Engineering, Donghua University, Shanghai 201620, China
[b] College of Textiles and Clothing, Wuyi University, Jiangmen 529020, Guangdong, China
[c] College of Textiles, Donghua University, Shanghai 201620, China
[d] Nanomaterials Research Center, Modern Textile Institute, Donghua University, Shanghai 200051, China

ARTICLE INFO

Article history:
Received 30 November 2013
Received in revised form 15 February 2014
Accepted 28 February 2014
Available online 12 March 2014

Keywords:
Nanofiber-net-binary structure
Chitosan
Polyethyleneimine
Formaldehyde detection

ABSTRACT

Here we describe a formaldehyde sensor fabricated by coating polyethyleneimine (PEI) functionalized chitosan nanofiber-net-binary structured layer on quartz crystal microbalance (QCM). The chitosan fibrous substrate comprising nanofibers and spider-web-like nano-nets constructed by a facile electrospinning/netting process provided an ideal structure for the uniform PEI modification and sensing performance enhancement. Benefiting from the fascinating nanostructure, abundant primary amine groups of PEI, and strong adhesive force to the QCM electrode of PEI–chitosan membranes, the developed formaldehyde sensor presented rapid response and low detection limit (5 ppm) at room temperature. These findings have important implications in fabricating multi-dimensional nanostructures on QCM for gas sensing and chemical analysis.

1. Introduction

Formaldehyde, as a ubiquitous air pollutant in the environment, has attracted emerging attention during the past few years. Particularly, formaldehyde emitted from the household products has become a persisting problem and caused a long lasting danger to human health (Chung, Tzeng, Ke, & Lee, 2013; Noguchi, Fujishima, Sawunyama, & Hashimoto, 1998; Sexton et al., 2004). Due to the toxicity and volatility of formaldehyde, various analytical methods have been developed for the detection of formaldehyde in the past decades (Flueckiger, Ko, & Cheung, 2009; Ho & Yu, 2003; Pang & Lewis, 2012). However, most of these techniques require sophisticated equipment, and generally are expensive and time consuming. Without doubt, it is highly desirable to develop a sensitive and easy-to-use method for formaldehyde detection.

Quartz crystal microbalance (QCM) has been widely used due to its accuracy, real-time detection and easy to use (Wang, Cui, Lin, Ding, Yu, & Al-Deyab, 2012). It is a room-temperature operated platform for mass sensing by the deposition of sensitive coatings, and the mass changes are directly related to the interaction between adsorption compounds and sensitive coating layers (Kimura et al., 2012; Wang, Raza, et al., 2012; Wang, Wang, Si, et al., 2012). Nanostructured materials, especially nanofibers, have received increasing attention for various applications due to their large surface area, high porosity and interconnected porous structures (Li et al., 2012; Luo et al., 2012; Wang, Ding, Yu, & Wang, 2011; Wang, Raza, Si, Yu, Sun, & Ding, 2013). Based on the characters mentioned above, considerable efforts have been devoted to develop nanofiber based QCM sensors to enhance the sensing performance (Virji, Kaner, & Weiller, 2006; Wang, Cui, et al., 2012).

Electro-spinning/netting (ESN) process, as a breakthrough in the field of electrospinning technique, has evoked much interest due to its ability to construct nanofibers-net-binary (NNB) structured membranes comprising one-dimensional (1D) nanofibers and two-dimensional spider-web-like nano-nets (Ding, Li, Miyauchi, Kuwaki, & Shiratori, 2006; Nirmala, Navamathavan, Kang, El-Newehy, & Kim, 2011; Wang, Ding, Sun, Wang, & Yu, 2013). The nano-nets could create enhanced interconnectivity and specific surface area and facilitate the diffusion of analytes into the NNB structured membranes, thus could be considered as attractive candidates as sensing substrate loaded with receptors for ultrasensitive QCM sensors. Up to now, we have obtained polyamide-6 (PA-6), polyaniline/PA-6, and polyacrylic acid NNB structured membranes and exploited their sensing performance

* Corresponding author at: State Key Laboratory for Modification of Chemical Fibers and Polymer Materials, College of Materials Science and Engineering, Donghua University, Shanghai 201620, China. Fax: +86 21 62378202.
E-mail addresses: binding75@yahoo.com, binding@dhu.edu.cn (B. Ding).

http://dx.doi.org/10.1016/j.carbpol.2014.02.088
0144-8617/

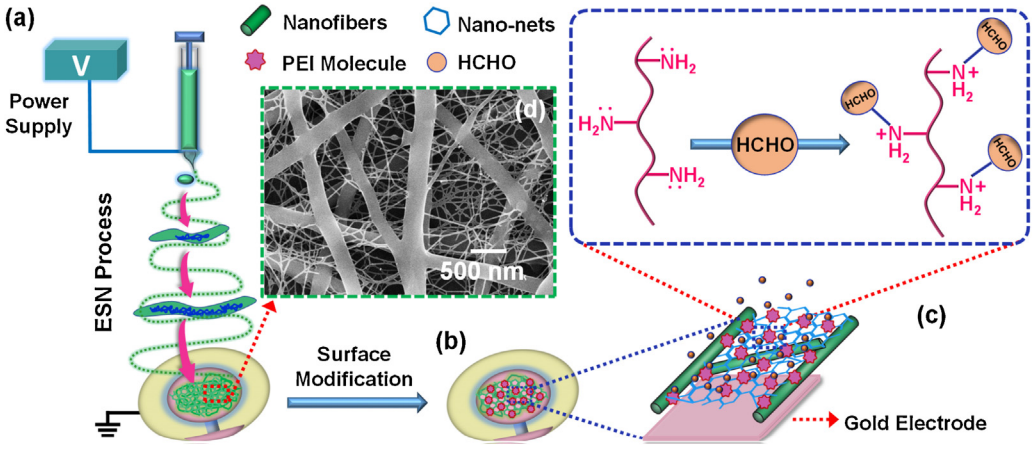

Fig. 1. Schematic diagram illustrating the fabrication of sensing layers on QCM. (a) ESN deposition of fibrous membranes onto the electrode of QCM. (b) Surface modification of NNB with diluted PEI solutions. (c) Illustration of PEI–chitosan fibers on gold electrode and the reaction mechanism between formaldehyde and PEI. (d) Typical FE-SEM image of NNB structured chitosan membranes.

to formaldehyde (Wang, Si, Wang, Ding, Yu, & Al-Deyab, 2012), HCl (Wang, Raza, et al., 2012; Wang, Wang, Si, et al., 2012), and humidity (Wang, Ding, Yu, Wang, & Pan, 2010), respectively.

Chitosan is generally derived from the alkaline deacetylation of chitin, one of nature's most abundant biopolymers (Desai, Kit, Li, & Zivanovic, 2008; Du & Hsieh, 2008; Muzzarelli, Boudrant, Meyer, Manno, DeMarchis, & Paoletti, 2012; Muzzarelli, 2012). It is mostly chosen as the starting polymer for the preparation of fibrous membranes owing to the enticing properties such as biocompatibility, biodegradability, and adsorption capabilities (Pakravan, Heuzey, & Ajji, 2011; Zhang et al., 2008). Until now, considerable efforts have been devoted to the variables in chitosan nanofibrous membranes (Homayoni, Ravandi, & Valizadeh, 2009; Ohkawa, Cha, Kim, Nishida, & Yamamoto, 2004; Su et al., 2011). However, to the best of our knowledge, no effort has been made to develop a promising strategy to combine polyethyleneimine (PEI) modified chitosan NNB membrane and QCM to construct highly sensitive formaldehyde sensors.

In this contribution, it is aimed to investigate the effects of solution properties on the fiber morphology of resultant chitosan membranes. The as-prepared chitosan membranes were further functionalized by sensing PEI (Fig. 1b). More significantly, the PEI modified chitosan membrane was used as a novel model on QCM for formaldehyde detection for the first time (Fig. 1c). This study is the initial motivation behind being a starting point of the development of QCM-based PEI–chitosan sensors for potential applications in routine formaldehyde detection.

2. Experimental

2.1. Materials

Chitosan (M_w = 210 kDa, the degree of deacetylation was 92%) was purchased from Yuhuan Ocean Biochemical Co., China, PEI (M_w = 70,000, Alfa Aesar Co., Ltd.) aqueous solution of 30 wt%, pure water with a resistance of 18.2 MΩ, formaldehyde (GCS grade), ethanol (95 wt%), acetic acid (99.5 wt%) and sodium dodecyl sulfate (SDS) were purchased from Aladdin Chemical Co., China. All chemicals were used as received without further purification.

2.2. Preparation of polymer solutions

Chitosan solutions were prepared at concentrations of 2, 3, and 4 wt% by dissolving in 90 wt% acetic acid with vigorous stirring. Chitosan/SDS blended solutions were obtained by adding different contents of SDS to chitosan solutions (4 wt%), respectively. The concentration of used SDS was 0.05, 0.1, and 0.2 wt%, respectively. PEI was diluted to 1 wt% with a pure water/ethanol weight ratio of 1:2. The ethanol was used to accelerate the diffusion process of PEI into NNB structured chitosan membranes.

2.3. Fabrication of fibrous membranes on QCM

The set-up for ESN deposition of NNB structured membranes on the electrode of QCM is depicted in Fig. 1a. The polymer solutions were loaded into a syringe that was attached to a high voltage power supply (DWP303-1ACD8) that was capable of generating voltages up to 30 kV. A syringe pump (LSP02-1B) was used to regulate the feed rate of the solutions at 0.5 mL h^{-1}. The ESN chamber was kept at a constant temperature of 25 °C with a relative humidity of 25%. The fibrous membranes were deposited on the grounded electrode of QCM (5 MHz, AT-cut quartz crystal with Au electrodes) at a 15 cm tip-to-collector distance until the required frequency shift was obtained. The resonance frequencies were measured by a QCM digital controller (QCM200, Stanford Research Systems). Fibrous membranes coated QCMs were dried at 25 °C in vacuum for 12 h prior to the subsequent characterizations.

2.4. Casting of PEI

PEI (1 wt%) solution was drop cast onto fibrous chitosan membranes by a micropipettor (5–50 ml, Shanghai Liansheng Instrumental Factory), through which fibrous PEI–chitosan membranes were prepared. After the solvents completely evaporated at room temperature, the membranes coated on QCM sensors were dried at 25 °C for 12 h in vacuum.

2.5. Measurement of sensing properties

The sensor was installed in the QCM testing chamber (7.64 L) which kept at the constant temperature of 23 °C and RH of 40%, respectively. A Hamilton microlitre syringe was used for formaldehyde injections. The concentration of injected formaldehyde in the chamber was calculated in ppm according to the following equation (Wang, Cui, et al., 2012):

$$C = \left(\frac{22.4\rho TV_s}{273MV}\right) \times 10^3$$

where C is the concentration of gaseous formaldehyde (ppm), ρ is the density of liquid formaldehyde (g/ml), T is the testing

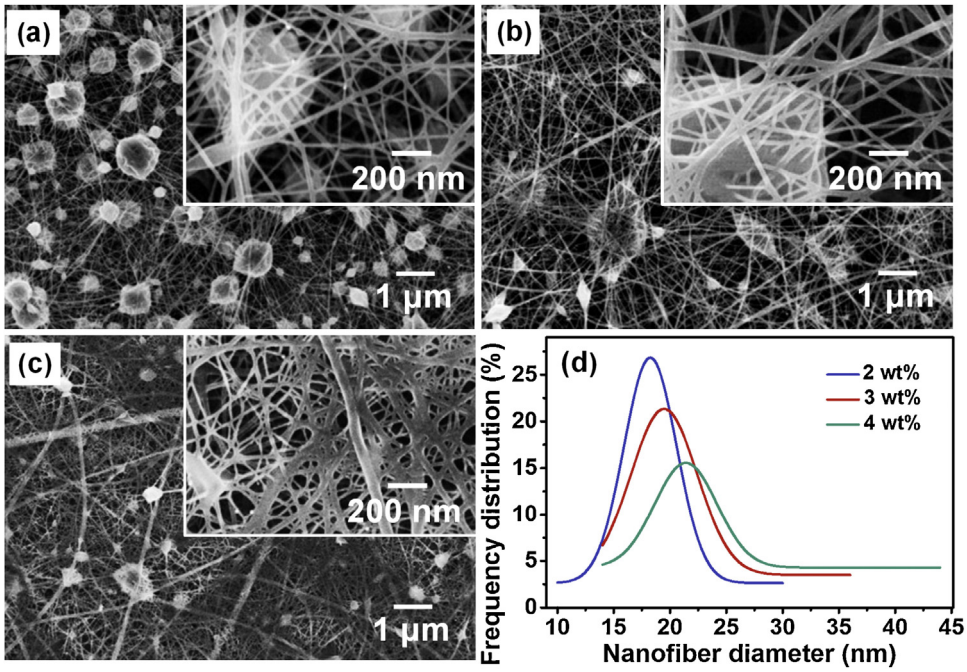

Fig. 2. FE-SEM images of chitosan nanofibrous membranes formed with a voltage of 30 kV, RH of 25% and various concentrations: (a) 2, (b) 3, and (c) 4 wt%. (d) Histogram showing the nanowire diameter distribution of nano-nets presented in relevant chitosan membranes.

temperature (Kelvin), V_s is the volume of formaldehyde (μL), M is the molecular weight of formaldehyde (g/mol), and V is the volume of the chamber (L). The sensing properties of the sensors were examined by measuring the resonance frequency shifts of QCM resulting from the additional mass loading. The resonance frequencies were measured by the frequency counter, and the data from the sensors were recorded by a personal computer (Wang, Raza, et al., 2012; Wang, Wang, Si, et al., 2012).

2.6. Characterization

The viscosity, conductivity and surface tension of chitosan solutions were measured by using a viscometer (CNDJ-79, Shanghai Changji Geological Instrument Co., Ltd., China), a conductivity meter (FE30, Mettler-Toledo Group, Switzerland) and an automatic surface tensiometer (QBZY-1, Shanghai Fangrui Instrument Co., Ltd., China), respectively. The morphology of fibrous membranes was characterized by field emission scanning electron microscopy (FE-SEM) (S-4800, Hitachi, Ltd., Japan). An image analyzer (Adobe Photoshop CS2) was applied to measure fiber diameters. Fourier transform infrared (FT-IR) spectra were recorded with a Nicolet 8700 FT-IR spectrometer in the range 4000–400 cm^{-1}. N_2 adsorption–desorption isotherms were examined at 77 K after pre-evacuation for 6 h at 323 K by an ASAP 2020 physisorption analyzer (Micromeritics, Co., USA).

3. Results and discussion

3.1. Morphological and structural characterization

The representative FE-SEM images of electrospun nanofibrous membranes fabricated by varying the concentration of chitosan are presented in Fig. 2a–c, revealing the typical three-dimensional (3D) nonwoven structure. As shown in Fig. 2a, the fibers formed from 2 wt% chitosan solution exhibited a bead-on-string structure, which contain thin fibers (average diameter of 18 nm) with numerous nano- to micro-sized beads along the fiber axis. The formation of this structure could be attributed to the utilization of the solutions with low viscosity and conductivity during the electrospinning process (Table 1). And the beads number reduced with increasing the concentration of chitosan solutions, but bead size increased slightly (Fig. 2b). Upon further increase of the chitosan concentration to 4 wt%, the beads-on-string structure disappeared, and resulted in the formation of homogeneous chitosan nanofibrous membranes with larger average nanofiber diameters (24 nm), as displayed in Fig. 2c and d. The phenomenon of bead-to-fiber transition could be explained from the aspect of chain entanglements in the polymer solutions. At lower concentrations (2 and 3 wt%), above the critical value, the chitosan chain overlaps of hydrodynamic volumes were confined, which could be reflected in the sharply increased viscosity and conductivity (Table 1). Thus, polymer solutions consisting of short range entangled networks are prone to generate small droplets and beaded fibers rather than uniform fiber. These results indicated that concentration was a key parameter in determining the morphology of chitosan membranes, and similar morphological changes have been reported in previous studies (Ohkawa, Cha, Kim, Nishida, & Yamamoto, 2004; Ohkawa, Minato, Kumagai, Hayashi, & Yamamoto, 2006; Wang, Raza, et al., 2012; Wang, Wang, Si, et al., 2012).

3.2. Effect of the SDS content on the morphology of chitosan membranes

Substantial studies have reported that additives can act as efficient elements in improving the morphology of electrospun nanofibers, and surfactants owing to their accessibility are widely used to create defect-free NNB structures to improve the substrate applications (Hu et al., 2011; Wang, Wang, Ding, Yu, & Sun, 2012). Herein, the effects of the SDS anionic surfactant concentration on the structure of chitosan nanofibrous membranes were evaluated systematically. Fig. 3 presents the FE-SEM images of the nanofibers fabricated from chitosan solutions containing various concentrations of SDS. Compared with the as-prepared pristine chitosan nanofibers (Fig. 2c), the chitosan membranes obtained from chitosan/SDS solutions showed slightly increased number of beads and multiscale structures among membranes,

Table 1
Solution properties of relevant chitosan solutions.

Sample	Concentration of chitosan (wt%)	Content of SDS (wt%)	Viscosity (cps)	Conductivity ($\mu S\,cm^{-1}$)	Surface tension ($mN\,m^{-1}$)
Chitosan-2	2	0	251.5	320.2	30.33
Chitosan-3	3	0	1100.7	465.67	29.9
Chitosan-4	4	0	2001.4	600.23	28.19
Chitosan-2/SDS-0.05	4	0.05	1990.56	638.67	28.14
Chitosan-2/SDS-0.1	4	0.1	1977.6	645.33	26.33
Chitosan-2/SDS-0.2	4	0.2	1965.13	678.2	23.58

which could be attributed to the decreased viscosity and sharply increased conductivity (Table 1). More interestingly, the formation of "spider-web-like" nano-nets was observed interspersing among the thin chitosan nanofibers. The nano-nets made of interlinked 1D nanowires (19.6 nm) were supported by conventional electrospun chitosan nanofibers (293.8 nm). It is worthy that the nano-nets showed weighted Steiner-tree structure, in which three neighboring nanowires form a three-way junction with angular symmetry (Ding et al., 2006). In terms of this observation, it is concluded that these NNB structures create enhanced additional surface area, thereby facilitating the diffusion of analysts into the membranes, which may be potentially useful for sensing materials.

By increasing the SDS contents (from 0.05 to 0.10 wt%), the chitosan nanofibers and nanowires exhibited decreased diameters of 247.2 and 16.8 nm (Fig. 3b and b′), respectively. Another interesting feature here is the coverage rate of the nano-nets in chitosan membranes significantly increased with increasing the SDS contents. This phenomenon could be illustrated from the perspective of the formation mechanism of the nano-nets. The instability of the Taylor cone induced by the high electric field results in the formation of the electrospray charged droplets (Wang, Ding, Yu, & Yang, 2011; Yang et al., 2011). The droplet was distorted and expanded into thin films due to the comprehensive effects of the forces (coulombic repulsion, electrostatic force, air resistance, gravity, surface tension, and viscoelastic force) during the flight process from the needle tip to the collector in the electrostatic field (Ding et al., 2006). The occurrence of rapid phase separation on splitting-film and the minimum energy principle may lead to the formation of nano-nets within milliseconds.

Further increase in the contents of SDS, individual surfactant monomers may bind together through the interaction between the charged head-group of SDS and the charged groups on the

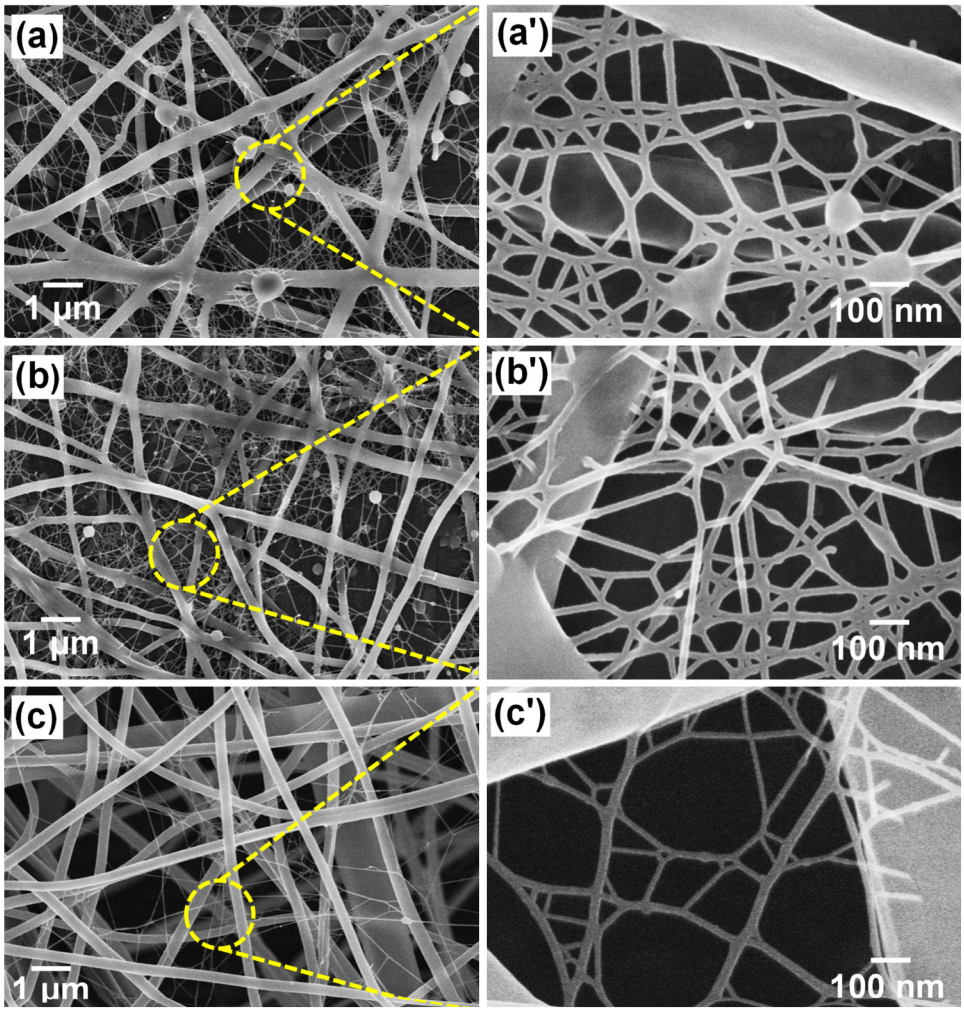

Fig. 3. FE-SEM images of chitosan NNB membranes formed with a voltage of 30 kV, RH of 25%, distance of 15 cm and various SDS concentrations: (a) 0.05, (b) 0.1, and (c) 0.2 wt%. (a′), (b′), and (c′) are the corresponding images at high magnification.

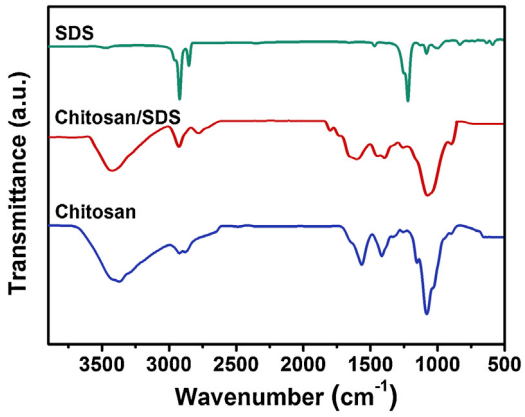

Fig. 4. FT-IR spectra of SDS powder, chitosan/SDS, and chitosan fibrous membranes.

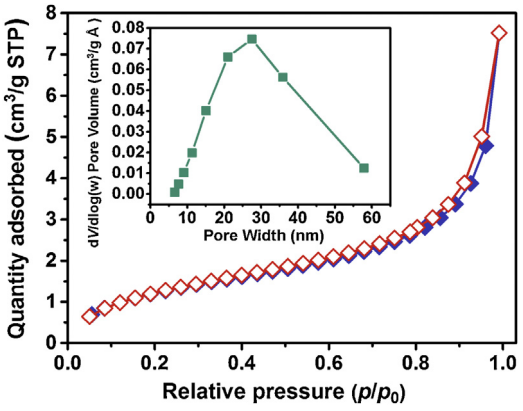

Fig. 5. Nitrogen adsorption–desorption isotherms of chitosan NNB membranes. Inset shows the pore distribution analysis of relevant chitosan membranes using BJH method.

chitosan chains, which may result in the increase of instability of the charged droplets and formation frequency of the nano-nets. Nevertheless, it is worth noting that the morphology of NNB structure obtained from chitosan/SDS (0.2 wt%) was not homogeneous, with greatly expanded pore-width (from 184 to 389 nm) and partly spilt nano-nets (Fig. 3c and c′), which could be attributed to the soluble single phase surfactant–polymer complexes driven by electrostatic attraction and the hydrophobic effect. As a consequence, chitosan/SDS membranes displayed a defective nanofibers morphology. The results in Fig. 3 indicated that surfactant is likely to be a primary factor that contributes to the regulation of the morphology of the NNB membranes.

3.3. FT-IR spectra

Evidence for the formation of NNB structured chitosan/SDS membranes comes from FT-IR spectral analysis (Fig. 4). In the case of SDS powder, the characteristic bands were observed at 2930 and 2847 cm^{-1}, corresponding to symmetric and asymmetric CH stretching. And the bands at 1469 and 1184 cm^{-1} are assigned to the bending mode of CH group and asymmetric S=O stretching, respectively (De Vasconcelos et al., 2006; Wan, Wu, Yu, & Wen, 2006). For the pure chitosan nanofibers, a broad band is observes in the range of 3250–3500 cm^{-1}, which could be attributed to N-H and OH···O stretching vibrations and intermolecular hydrogen bonding of the polysaccharide molecules (Pakravan, Heuzey, & Ajji, 2011). The two middle strong bands at 1646 and 1564 cm^{-1} are assigned to the carbonyl group C=O—NH or amide I band and the amine —NH_2 or amide II band, respectively. The peaks at 1413 and 1369 cm^{-1} belong to the deformation of C—CH_3 and the amide III band (Homayoni, Ravandi, & Valizadeh, 2009; Kriegel, Kit, McClements, & Weiss, 2009). And the bands at 1148, 1079, and 1028 cm^{-1} are assigned to showing the anti-symmetric stretching of the C—O—C bridge, skeletal vibrations involving C—O stretching, which presented the saccharide structure of chitosan (Kriegel, Kit, McClements, & Weiss, 2009). Fig. 4 shows an FT-IR spectrum of the as-prepared chitosan/SDS membranes. Besides the absorption features of SDS and chitosan, an obvious decrease in intensity of the amide I and II bands was observed, which suggests that the decrease in free chitosan molecules due to the formation of soluble single phase surfactant–polymer complexes, which indicates the existence of SDS in the NNB structured chitosan membranes.

3.4. Quantitative porous analysis of chitosan NNB membranes

The fascinating NNB structure of the chitosan membranes enabled us to deeply investigate their porous structure. The relevant N_2 adsorption–desorption isotherms curves displayed in Fig. 5 showed a series of typical adsorption behaviors of the isotherm of type IV, revealing the characteristics of mesopores within the as-prepared membranes. The narrow hysteresis loop in this region indicated that the mesopores are open, and no significant interruption between the capillary evaporation and condensation for N_2 (Li, Cao, Yin, Lu, & Yin, 2011; Si, Ren, Li, Ding, & Yu, 2012). Apart from that, detailed pore size distribution (PSD) analysis was achieved by employing the Barrett–Joyner–Halenda (BJH) method. As shown in Fig. 5 (inset), the chitosan membranes displayed the polydisperse porous structure and a primary PSD in the range of 15–55 nm. Taking advantage of the small pore size and high porosity, the NNB structured chitosan membranes possess numerous adsorption sites are appropriate to act as the template of QCM sensors, which could significant boost the interactions between formaldehyde molecules and sensing materials (Wang, Raza, et al., 2012; Wang, Wang, Si, et al., 2012).

3.5. Morphology of PEI modified NNB membranes

The FE-SEM images of chitosan membranes modified by PEI are exhibited in Fig. 6. After the modification of PEI, the 3D porous fibrous structure and the NNB structure of chitosan membranes are still maintained in the PEI–chitosan composite fibers (Fig. 6a and a′). It is clearly seen that the sensing PEI was not only adsorbed on the surface of the NNB structured chitosan membranes, but also penetrated into the interspaces among the nanofibers and nano-nets and formed the conglutination phenomenon. As a result, the connection between sensing membranes and QCM electrode was further enhanced and the stability of the sensing layers was also improved, making this structure useful in practical electronic device applications (Wang, Cui, et al., 2012).

3.6. Formaldehyde gas sensing performance

The formaldehyde sensing properties of PEI-modified NNB structured chitosan fibers on QCM were investigated by measuring the frequency shifts when the fibrous membranes were exposed to formaldehyde vapors. During the process of exposure, the sensor responses (ΔF) for each formaldehyde concentration were obtained from the frequency alternations between the corresponding frequencies at the beginning and the end of the exposure process (Wang, Raza, et al., 2012; Wang, Wang, Si, et al., 2012). Fig. 7a presents the frequency response of QCM-based chitosan NNB sensors with various PEI coating loads upon sequential exposure as a function of formaldehyde concentration (5, 15, 35, 85, and 185 ppm) in a temperature controlled measurement cell. The

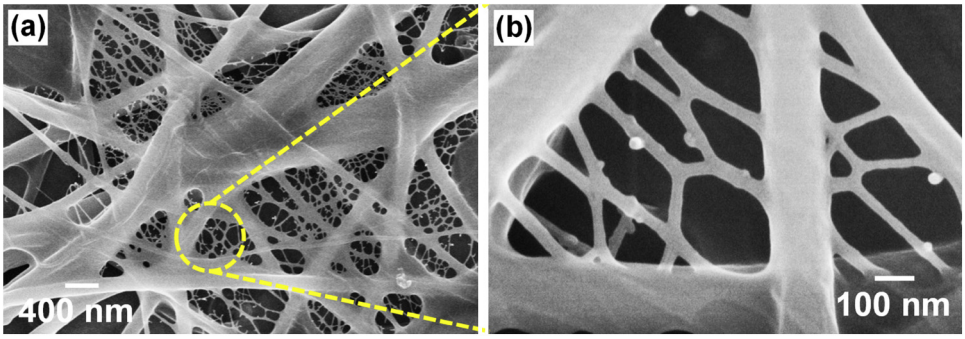

Fig. 6. FE-SEM images of PEI modified chitosan membranes.

QCM sensor coated with only NNB structured chitosan fibers exhibited a slightly response (ΔF = 0.06 Hz) upon exposure to 5 ppm of formaldehyde. The ΔF of the chitosan fibers coated QCM sensors exposed to 15, 35, 85, and 185 ppm of formaldehyde were 0.23, 1.08, 2.04, and 4.3 Hz, respectively. It is clearly seen that the response amplitude of the sensors increased gradually with increasing the formaldehyde concentration. This phenomenon could be attributed to the moisture absorbed on NNB structured chitosan fibers, which allow for easy diffusion of formaldehyde molecules into the sensing layers.

QCM based PEI–chitosan sensors with PEI coating loads of 1500 and 8000 Hz showed a rapid response and reached higher ΔF (0.57 and 0.95 Hz) upon exposure 5 ppm formaldehyde. Besides, QCM-based PEI–chitosan sensors with PEI coating load of 8000 Hz presented the fastest response speed among the three samples. When the PEI–chitosan sensors were exposed to 185 ppm of formaldehyde, the ΔF of the sensors with different PEI coating loads (0, 1500, and 8000 Hz) were 4.3, 14.58, and 31.92 Hz, respectively. Evidently, QCM-based PEI–chitosan sensors with PEI coating load of 8000 Hz has achieved the best sensing properties toward the accumulated formaldehyde concentrations, approximately seven times as much as a chitosan fiber coated sensor. These results could be attributed to the nucleophilic addition interaction between the formaldehyde and the amine groups of PEI molecules, as well as the NNB structure of chitosan membranes. Fig. 7b displays the ΔF values of QCM-based PEI–chitosan sensors with different PEI coating loads (0, 1500, and 8000 Hz) in sensing formaldehyde with concentrations of 5–185 ppm. The QCM isotherm to formaldehyde shows a Henry-type sorption in the concentration range (Kimura et al., 2012). The above sorption behavior was also observed in the QCM response of fibrous PEI/poly(vinyl alcohol) and PEI/titanium dioxide membranes (Wang, Cui, et al., 2012; Wang, Ding, Sun, Yu, & Sun, 2010).

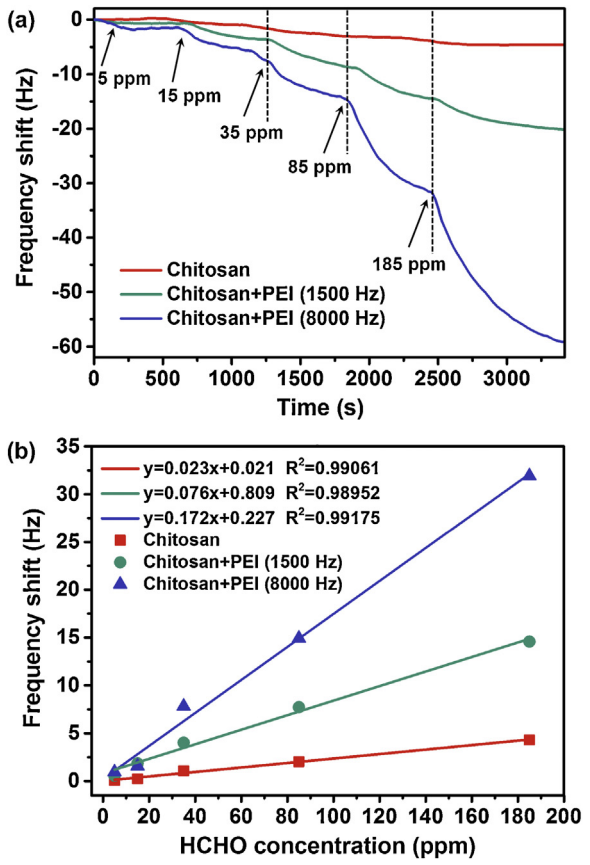

Fig. 7. Response of QCM-based PEI–chitosan sensors with various PEI coating loads (0, 1500, and 8000 Hz) upon exposure to increasing formaldehyde concentrations (5–185 ppm) at ambient temperature of 25 °C. (b) The frequency shift versus formaldehyde concentration. The coating load of chitosan was 2000 Hz.

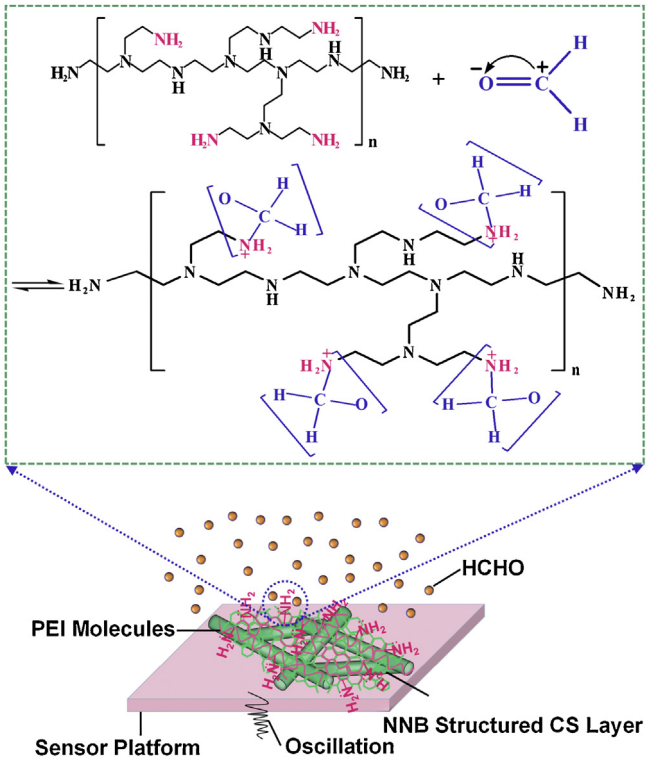

Fig. 8. Schematic representation of formaldehyde vapor detecting mechanism based on chitosan membranes.

3.7. Sensing mechanism

Based on the formaldehyde sensing properties of QCM based PEI–chitosan sensors, we concluded the following two outstanding advantages of NNB structured PEI–chitosan sensors. On one hand, the unique structure and high porous configuration of NNB membranes are beneficial to achieve high and rapid response via effective and quick diffusion of analyst vapor. The NNB structured PEI–chitosan layer could provide increased diffusion paths for the formaldehyde molecules, enhancing the vapor diffusion and mass transportation in sensing material. Additionally, the large packing density of chitosan NNB membranes also facilitated the oscillation transmission to a great extent, resulting in much faster response.

On the other hand, the reversible nucleophilic addition chemical reaction between formaldehyde molecules and primary amine groups of PEI could lead to the formaldehyde molecules adsorbed onto the surface of sensing layers (Fig. 8). Therefore, the number of primary amine groups of PEI was the key point in determining the sensing performance of QCM sensors (Wang, Cui, et al., 2012; Zhang et al., 2010), which was also demonstrated in this contribution that the increased coating load of PEI led to the improvement of sensitivity. Moreover, the reversible reaction between formaldehyde molecules and primary amine groups of PEI supplied the reproducibility of the resultant QCM based PEI–chitosan sensors. All the above implied that the QCM based PEI–chitosan structured sensors could be potentially used to monitor formaldehyde in indoor air.

4. Conclusions

In summary, we have described the fabrication of a novel PEI functionalized chitosan NNB membrane on QCM for formaldehyde detection. The morphology of the NNB architecture of chitosan is controllable and the final morphology is highly dependent on the concentration of solutions and the SDS contents. Chitosan/SDS (0.1 wt%) solutions formed the optimal NNB structured membranes with a specific surface area of 8.25 g/m^2 and high porosity, which enlarged the sensing area and thus facilitated the diffusion of formaldehyde into the PEI modified sensing layers. Gas sensing performance indicated that the as-prepared QCM sensor showed high sensitivity and a low-level detection limit (5 ppm) for formaldehyde, indicating their promising application in the detection of trace formaldehyde in the environment. Moving forward, this work also promotes a strategy for the design and development of the NNB structured membrane based highly sensitive sensors toward various analytes in the future.

Acknowledgements

This work is supported by the National Natural Science Foundation of China (Nos. 51173022, 51273038 and 51322304), the Shanghai Nano Special Projects (11nm0502900), the Program for New Century Talents of the University in China, the Fundamental Research Funds for the Central Universities, and the “DHU Distinguished Young Professor Program”.

References

Chung, P. R., Tzeng, C. T., Ke, M. T., & Lee, C. Y. (2013). Formaldehyde gas sensors: A review. *Sensors*, *13*(4), 4468–4484.

De Vasconcelos, C. L., Bezerril, P. M., Dos Santos, D. E. S., Dantas, T. N. C., Pereira, M. R., & Fonseca, J. L. C. (2006). Effect of molecular weight and ionic strength on the formation of polyelectrolyte complexes based on poly(methacrylic acid) and chitosan. *Biomacromolecules*, *7*(4), 1245–1252.

Desai, K., Kit, K., Li, J., & Zivanovic, S. (2008). Morphological and surface properties of electrospun chitosan nanofibers. *Biomacromolecules*, *9*(3), 1000–1006.

Ding, B., Li, C. R., Miyauchi, Y., Kuwaki, O., & Shiratori, S. (2006). Formation of novel 2D polymer nanowebs via electrospinning. *Nanotechnology*, *17*(15), 3685–3691.

Du, J., & Hsieh, Y. L. (2008). Nanofibrous membranes from aqueous electrospinning of carboxymethyl chitosan. *Nanotechnology*, *19*(12), 125707.

Flueckiger, J., Ko, F., & Cheung, K. (2009). Microfabricated formaldehyde gas sensors. *Sensors*, *9*(11), 9196–9215.

Ho, S. S. H., & Yu, J. Z. (2003). Determination of airborne carbonyls: Comparison of a thermal desorption/GC method with the standard DNPH/HPLC method. *Environmental Science and Technology*, *38*(3), 862–870.

Homayoni, H., Ravandi, S. A. H., & Valizadeh, M. (2009). Electrospinning of chitosan nanofibers: Processing optimization. *Carbohydrate Polymers*, *77*(3), 656–661.

Hu, J., Wang, X., Ding, B., Lin, J., Yu, J., & Sun, G. (2011). One-step electro-spinning/netting technique for controllably preparing polyurethane nano-fiber/net. *Macromolecular Rapid Communications*, *32*(21), 1729–1734.

Kimura, M., Sakai, R., Sato, S., Fukawa, T., Ikehara, T., Maeda, R., et al. (2012). Sensing of vaporous organic compounds by TiO_2 porous films covered with polythiophene layers. *Advanced Functional Materials*, *22*(3), 469–476.

Kriegel, C., Kit, K. M., McClements, D. J., & Weiss, J. (2009). Electrospinning of chitosan–poly(ethylene oxide) blend nanofibers in the presence of micellar surfactant solutions. *Polymer*, *50*(1), 189–200.

Li, B., Cao, H., Yin, G., Lu, Y., & Yin, J. (2011). Cu_2O@reduced graphene oxide composite for removal of contaminants from water and supercapacitors. *Journal of Materials Chemistry*, *21*(29), 10645–10648.

Li, Y., Xiao, W., Xiao, K., Berti, L., Luo, J., Tseng, H. P., et al. (2012). Well-defined, reversible boronate crosslinked nanocarriers for targeted drug delivery in response to acidic pH values and cis-Diols. *Angewandte Chemie International Edition*, *51*(12), 2864–2869.

Luo, H., Jiang, B., Li, B., Li, Z., Jiang, B., & Chen, Y. C. (2012). Kaempferol nanoparticles achieve strong and selective inhibition of ovarian cancer cell viability. *International Journal of Nanomedicine*, *7*, 3951–3959.

Muzzarelli, R. A. A., Boudrant, J., Meyer, D., Manno, N., DeMarchis, M., & Paoletti, M. G. (2012). Current views on fungal chitin/chitosan, human chitinases, food preservation, glucans, pectins and inulin: A tribute to Henri Braconnot, precursor of the carbohydrate polymers science, on the chitin bicentennial. *Carbohydrate Polymers*, *87*(2), 995–1012.

Muzzarelli, R. A. A. (2012). Nanochitins and nanochitosans, paving the way to eco-friendly and energy-saving exploitation of marine resources. *Polymer Science: A Comprehensive Reference*, *10*, 153–164.

Nirmala, R., Navamathavan, R., Kang, H. S., El-Newehy, M. H., & Kim, H. Y. (2011). Preparation of polyamide-6/chitosan composite nanofibers by a single solvent system via electrospinning for biomedical applications. *Colloids and Surfaces B: Biointerfaces*, *83*(1), 173–178.

Noguchi, T., Fujishima, A., Sawunyama, P., & Hashimoto, K. (1998). Photocatalytic degradation of gaseous formaldehyde using TiO_2 film. *Environmental Science and Technology*, *32*(23), 3831–3833.

Ohkawa, K., Cha, D., Kim, H., Nishida, A., & Yamamoto, H. (2004). Electrospinning of chitosan. *Macromolecular Rapid Communications*, *25*(18), 1600–1605.

Ohkawa, K., Minato, K. I., Kumagai, G., Hayashi, S., & Yamamoto, H. (2006). Chitosan nanofiber. *Biomacromolecules*, *7*(11), 3291–3294.

Pakravan, M., Heuzey, M. C., & Ajji, A. (2011). A fundamental study of chitosan/PEO electrospinning. *Polymer*, *52*(21), 4813–4824.

Pang, X., & Lewis, A. C. (2012). A microfluidic lab-on-chip derivatisation technique for the measurement of gas phase formaldehyde. *Analytical Methods*, *4*(7), 2013–2020.

Sexton, K., Adgate, J. L., Mongin, S. J., Pratt, G. C., Ramachandran, G., Stock, T. H., et al. (2004). Evaluating differences between measured personal exposures to volatile organic compounds and concentrations in outdoor and indoor air. *Environmental Science and Technology*, *38*(9), 2593–2602.

Si, Y., Ren, T., Li, Y., Ding, B., & Yu, J. (2012). Fabrication of magnetic polybenzoxazine-based carbon nanofibers with Fe_3O_4 inclusions with a hierarchical porous structure for water treatment. *Carbon*, *50*(14), 5176–5185.

Su, P., Wang, C., Yang, X., Chen, X., Gao, C., Feng, X. X., et al. (2011). Electrospinning of chitosan nanofibers: The favorable effect of metal ions. *Carbohydrate Polymers*, *84*(1), 239–246.

Virji, S., Kaner, R. B., & Weiller, B. H. (2006). Hydrogen sensors based on conductivity changes in polyaniline nanofibers. *Journal of Physical Chemistry B*, *110*(44), 22266–22270.

Wan, Y., Wu, H., Yu, A., & Wen, D. (2006). Biodegradable polylactide/chitosan blend membranes. *Biomacromolecules*, *7*(4), 1362–1372.

Wang, J., Raza, A., Si, Y., Cui, L., Ge, J., Ding, B., et al. (2012). Synthesis of super-amphiphobic breathable membranes utilizing SiO_2 nanoparticles decorated fluorinated polyurethane nanofibers. *Nanoscale*, *4*(23), 7549–7556.

Wang, N., Raza, A., Si, Y., Yu, J., Sun, G., & Ding, B. (2013). Tortuously structured polyvinyl chloride/polyurethane fibrous membranes for high-efficiency fine particulate filtration. *Journal of Colloid and Interface Science*, *398*, 240–246.

Wang, N., Wang, X., Ding, B., Yu, J., & Sun, G. (2012). Tunable fabrication of three-dimensional polyamide-66 nano-fiber/nets for high efficiency fine particulate filtration. *Journal of Materials Chemistry*, *22*(4), 1445–1452.

Wang, X., Cui, F., Lin, J., Ding, B., Yu, J., & Al-Deyab, S. S. (2012). Functionalized nanoporous TiO_2 fibers on quartz crystal microbalance platform for formaldehyde sensor. *Sensors and Actuators B: Chemical*, *171–172*, 658–665.

Wang, X., Ding, B., Sun, G., Wang, M., & Yu, J. (2013). Electro-spinning/netting: A strategy for the fabrication of three-dimensional polymer nano-fiber/nets. *Progress in Materials Science*, *58*(8), 1173–1243.

Wang, X., Ding, B., Sun, M., Yu, J., & Sun, G. (2010). Nanofibrous polyethyleneimine membranes as sensitive coatings for quartz crystal microbalance-based formaldehyde sensors. *Sensors and Actuators B: Chemical*, *144*(1), 11–17.

Wang, X., Ding, B., Yu, J., & Wang, M. (2011). Engineering biomimetic superhydrophobic surfaces of electrospun nanomaterials. *Nano Today*, *6*(5), 510–530.

Wang, X., Ding, B., Yu, J., & Yang, J. (2011). Large-scale fabrication of two-dimensional spider-web-like gelatin nano-nets via electro-netting. *Colloids and Surfaces B: Biointerfaces*, *86*(2), 345–352.

Wang, X., Si, Y., Wang, J., Ding, B., Yu, J., & Al-Deyab, S. S. (2012). A facile and highly sensitive colorimetric sensor for the detection of formaldehyde based on electro-spinning/netting nano-fiber/nets. *Sensors and Actuators B: Chemical*, *163*(1), 186–193.

Wang, X., Wang, J., Si, Y., Ding, B., Yu, J., Sun, G., et al. (2012). Nanofiber-net-binary structured membranes for highly sensitive detection of trace HCl gas. *Nanoscale*, *4*(23), 7585–7592.

Wang, X., Ding, B., Yu, J., Wang, M., & Pan, F. (2010). A highly sensitive humidity sensor based on a nanofibrous membrane coated quartz crystal microbalance. *Nanotechnology*, *21*(5), 055502.

Yang, S., Wang, X., Ding, B., Yu, J., Qian, J., & Sun, G. (2011). Controllable fabrication of soap-bubble-like structured polyacrylic acid nano-nets via electro-netting. *Nanoscale*, *3*, 564–568.

Zhang, C., Wang, X., Lin, J., Ding, B., Yu, J., & Pan, N. (2010). Nanoporous polystyrene fibers functionalized by polyethyleneimine for enhanced formaldehyde sensing. *Sensors and Actuators B: Chemical*, *3*, 1258–1262.

Zhang, Y., Venugopal, J. R., El-Turki, A., Ramakrishna, S., Su, B., & Lim, C. T. (2008). Electrospun biomimetic nanocomposite nanofibers of hydroxyapatite/chitosan for bone tissue engineering. *Biomaterials*, *29*(32), 4314–4322.